Electronic Supplementary Material (ESI) for Nanoscale.

Supplementary Information

for

Ion transport across solid-state ion channels perturbed by directed strain

A. Smolyanitsky, A. Fang, A.F. Kazakov, E. Paulechka

S1. DDAP atomic charges: anisotropic permeation across N_4O_2 pores and charge value dependence on strain

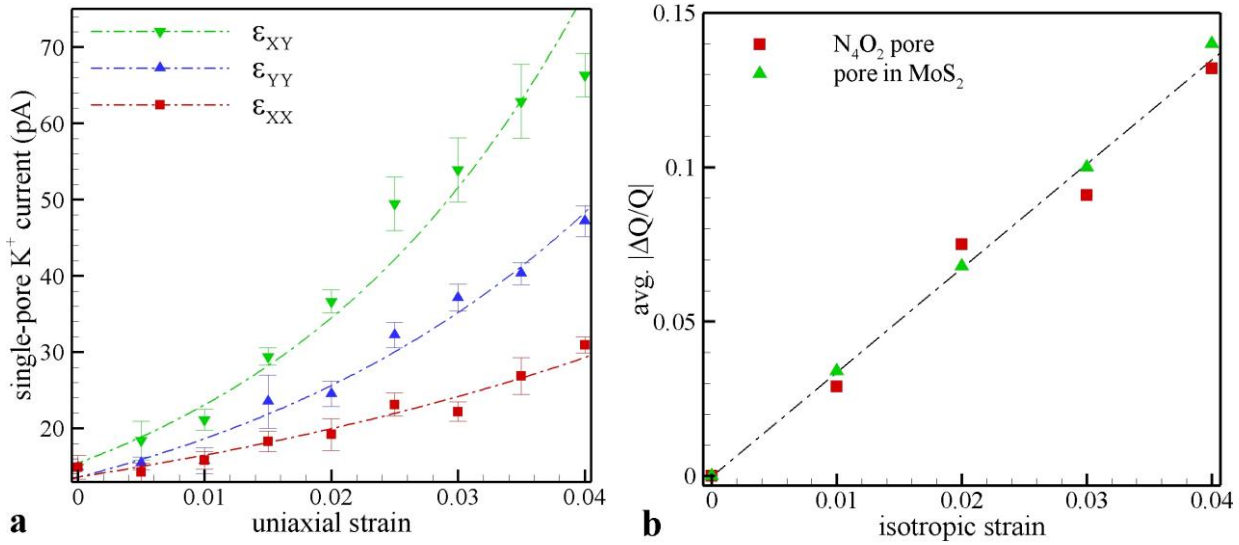

Figure S1. Analog of Fig. 2 in the main text, as obtained with DDAP charges (Q_O = -0.23, Q_N = -0.48) (a) and relative changes in DDAP atomic charges (averaged throughout the corresponding set of atoms lining each pore) as functions of isotropic strain (b). In (a), the strain sensitivities are $\mu_{XX} = 19.14$, $\mu_{YY} = 31.74$, and $\mu_{XY} = 48.03$ (μ_{XY} is obtained from exponential fitting to the data corresponding to $\varepsilon \leq 0.025$). In (b), atomic charges tend to *decrease* (in absolute value) with increasing strain.

S2. Analytical estimates of permeation anisotropy

The level of anisotropy in ionic permeability gated by uniaxial strains can be roughly estimated analytically. In the simplest case of X and Y strain directions, consider the structure in Fig. 1. The free energy for a pore-trapped solvated ion interacting with the hydrated pore is approximated as [1]:

$$U = U_{ion-pore} + U_{ion-water}, \qquad \text{(S1)}$$

where $U_{ion-pore} \propto \sum \left(\frac{Q_i}{r_0} - 2\frac{Q_i/2}{r_1} \right)$ is the sum of vacuum interactions with six edge dipoles (indexed by *i*) shown in Fig. 1. Here, each dipole consists of the negative atomic charge $-Q_i$ of the nitrogen or oxygen atom at the inner edge of the pore and a corresponding pair of carbons with charges $\frac{+Q_i}{2}$ at the outer edge. The following estimate does not include anisotropy in the changes $U_{ion-water}$ between Y and X directions and is limited to estimating the $\delta U_{ion-pore}^{YY} - \delta U_{ion-pore}^{XX}$ in the differential limit of pore geometry distortions, assuming that all atomic displacements due to strain correspond to bulk continuum values and ignoring the mechanical properties of the pore region. Also, only first-order electrostatic energy terms are included in the calculations. Just like in our MD simulations, we assume that the atomic charge values remain

constant with respect to bond stretching considered here. Given these assumptions, the following is a simple exposition of the main source of anisotropy and not a quantitative estimate.

For simplicity, absolute values of atomic charges are used below.

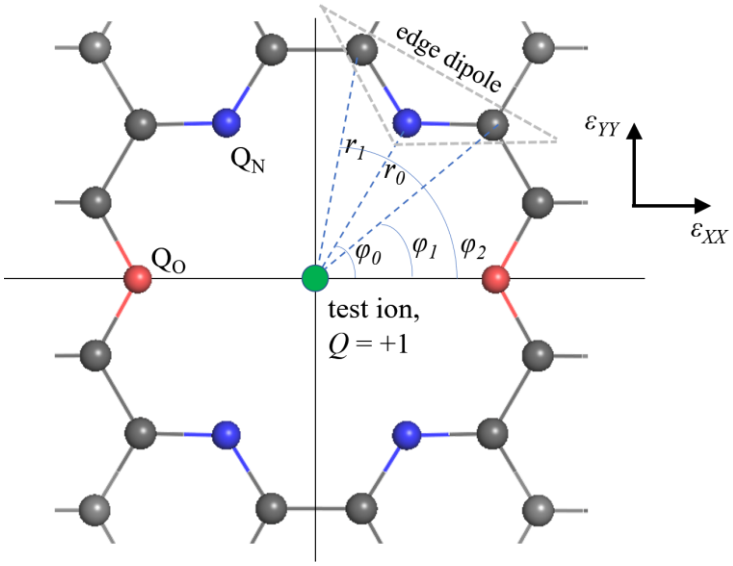

Figure S2. A positively charged test ion in an N_4O_2 crown-like pore subject to uniaxial strain along X or Y direction.

In general, for an arbitrary uniaxial strain direction, the change in $U_{ion-pore}$ is effectively the corresponding sum of tensor elements describing the changes in r_0 and r_1 for all dipoles interacting with the test ion in Fig. S2. With pore geometry in Fig. 1, each element can be estimated directly. For any membrane atom in the absence of strain interacting with the test ion at a distance r with the corresponding radius-vector $\boldsymbol{r}$ forming an angle φ with the X-direction, the radii perturbed by small uniaxial strains ε_{XX} and ε_{YY} are, respectively:

$$r_{XX} \approx r(1 + \varepsilon_{XX}\, cos^2\varphi),\ r_{YY} \approx r(1 + \varepsilon_{YY}\, sin^2\varphi). \qquad \text{(S2)}$$

For uniaxial ε_{YY}, all inner edge N atoms are vertically displaced, along with the corresponding outer-edge carbons, above and below Y = 0. The two O atoms remain unperturbed, while the corresponding carbons are displaced. The resulting change in energy is

$$\delta U^{YY}_{ion-pore} \propto \frac{3Q_N}{r_0}\varepsilon_{YY} - \frac{39}{14}\frac{Q_N}{r_1}\varepsilon_{YY} - \frac{3}{14}\frac{Q_O}{r_1}\varepsilon_{YY}. \qquad \text{(S3)}$$

For uniaxial ε_{XX}, all inner and outer atoms are displaced horizontally to the left and right of X = 0, so that:

$$\delta U^{XX}_{ion-pore} \propto \frac{Q_N}{r_0}\varepsilon_{XX} - \frac{17}{14}\frac{Q_N}{r_1}\varepsilon_{XX} + \frac{2Q_O}{r_0}\varepsilon_{XX} - \frac{25}{14}\frac{Q_O}{r_1}\varepsilon_{XX}. \qquad \text{(S4)}$$

As a sanity check, adding Eqs. (S3) and (S4), we obtain the correct energy change in response to biaxial strain. Assuming equal uniaxial strain magnitudes $\varepsilon_{YY} = \varepsilon_{XX} = \varepsilon$, we obtain:

$$\delta U_{ion-pore}^{YY} - \delta U_{ion-pore}^{XX} \propto \frac{2(Q_N - Q_O)}{r_0}\varepsilon - \frac{11}{7}\frac{(Q_N - Q_O)}{r_1}\varepsilon =$$

$$= 2(Q_N - Q_O)\left(\frac{1}{r_0} - \frac{1}{r_1}\right)\varepsilon + \frac{3}{7}\frac{(Q_N - Q_O)}{r_1}\varepsilon. \quad \text{(S5)}$$

Eq. (S5) without the rightmost term sets the following lower limit on the anisotropy in energy:

$$\delta U_{ion-pore}^{YY} - \delta U_{ion-pore}^{XX} \propto 2(Q_N - Q_O)\left(\frac{1}{r_0} - \frac{1}{r_1}\right)\varepsilon. \quad \text{(S6)}$$

Note that the right side of Eq. (S6) is conveniently equal to 1/3 of the change in total energy of ion-pore interaction in a *fully axisymmetric hexagonal pore lined with atoms carrying charge* $(Q_N - Q_O)$, subject to isotropic biaxial strain ε. This finding enables a rough numerical estimate.

To proceed from proportionality to functional dependence, we use the results in Ref. [1] to estimate the per-atom strain susceptibility $\mu_a \propto \left(\frac{1}{r_0} - \frac{1}{r_1}\right)$. From Fig. 4a therein, 2% of isotropic strain applied to a fully symmetric hexagonal pore lined with six oxygen atoms (crown $|Q_O|$ = 0.4) results in ~$6k_bT$ = 15 kJ/mol change in the ion-pore electrostatic energy. Thus, *per unit of strain, per unit of charge of the inner edge atom*, the susceptibility is μ_a = 750. The ion-pore energy anisotropy is therefore *at least*

$$\delta U_{ion-pore}^{YY} - \delta U_{ion-pore}^{XX} = \frac{\mu_a k_b T}{3}(Q_N - Q_O)\varepsilon. \quad \text{(S7)}$$

Finally, we correct for the Poisson effect and introduce Poisson's ratio υ = 0.19 [2], corresponding to bulk graphene with ripples significantly suppressed by water. The reader is encouraged to confirm that after simple manipulations Eq. (S7) becomes

$$\delta U_{ion-pore}^{YY} - \delta U_{ion-pore}^{XX} = \frac{\mu_a k_b T}{3}(1 - \upsilon)(Q_N - Q_O)\varepsilon. \quad \text{(S7a)}$$

A comparison between MD-simulated data and Eq. (S7a) is shown in Fig. S3.

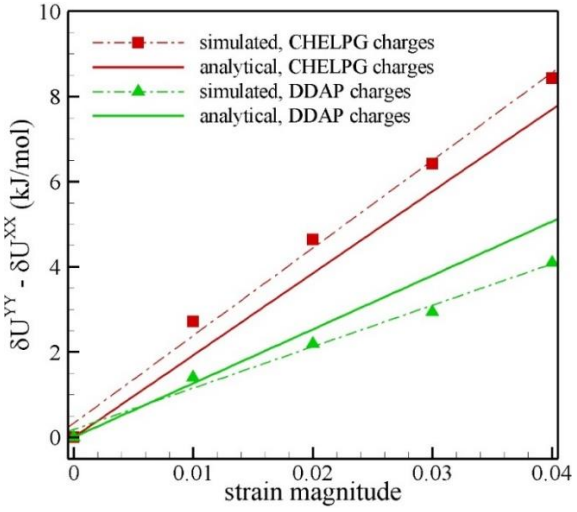

Figure S3. Simulated $\left(\delta U_{ion-pore}^{YY} - \delta U_{ion-pore}^{XX}\right)$ alongside the estimates by Eq. (S7a). The data is presented for CHELPG and DDAP atomic charge sets.

S3. Ion-water coordination

The coordination numbers are calculated as follows: $N_c = 4\pi \int_0^{r_1} g(r) r^2 dr$, where $r_1 = 0.36$ nm approximately corresponds to the first hydration shell. Here, $g(r)$ is the ion-water-oxygen radial distribution function (RDF). Shown in Fig. S4 are representative examples of MD-simulated RDF curves for a K^+ ion in bulk water and the same ion trapped in the unstrained N_4O_2 pore, as well as this pore subject to $\varepsilon_{YY} = \varepsilon_{XX} = 0.04$ in the presence of water.

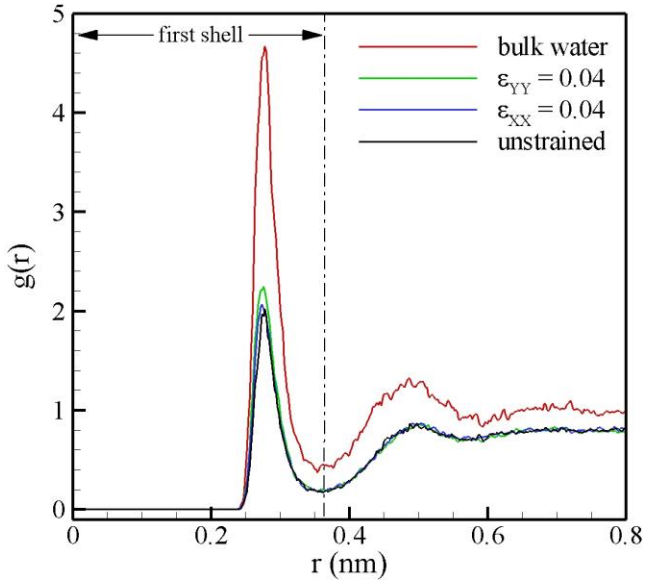

Figure S4. Examples of normalized ion-water-oxygen RDFs for K^+ ions in bulk water and in strained and unstrained N_4O_2 pores (each RDF is calculated from 2500 timeframes in a 50-ns-long simulation). As calculated, $N_{c,bulk} = 6.95$.

S4. Uniaxial strain applied along an arbitrary direction using a triclinic simulation cell

Here, a uniaxial strain of magnitude ε is directed at an angle φ with the X-axis. In the following, we find the parameters that define the triclinic cell of the strained system and the transformed initial coordinates of the atoms in the triclinic system (see Fig. S5). The following should be applicable to any simulation cell setup for the Gromacs simulation package.

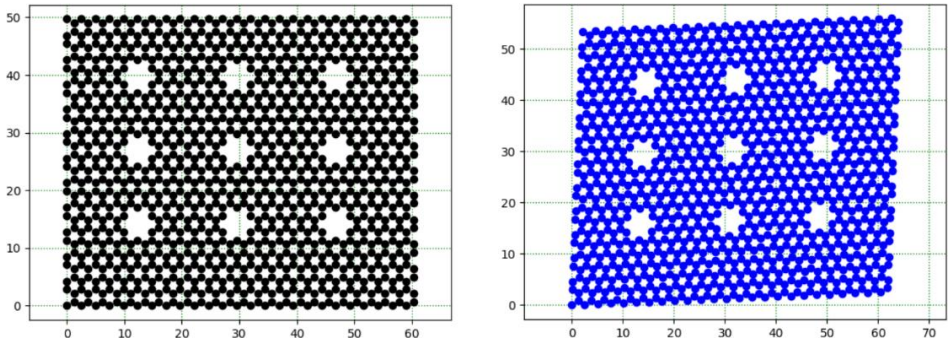

Figure S5. Example unstrained and strained triclinic system. The dimensions are in angstroms.

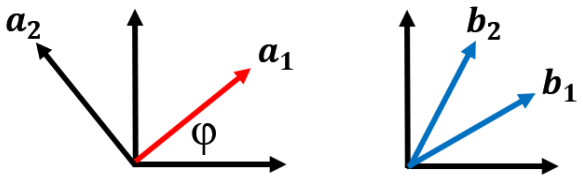

Figure S6. Vector definitions; strain is applied along $\boldsymbol{a_1}$.

The strain tensor converted from the basis oriented along the direction of uniaxial strain to the original coordinate axes is:

$$\begin{bmatrix} \varepsilon_{XX} & \varepsilon_{XY} \\ \varepsilon_{XY} & \varepsilon_{YY} \end{bmatrix}_O = \begin{bmatrix} cos\varphi & sin\varphi \\ -sin\varphi & cos\varphi \end{bmatrix} \begin{bmatrix} \varepsilon & 0 \\ 0 & 0 \end{bmatrix}_A \begin{bmatrix} cos\varphi & -sin\varphi \\ sin\varphi & cos\varphi \end{bmatrix} = \quad \text{(S9)}$$

$$= \begin{bmatrix} \varepsilon\, cos^2\varphi & \varepsilon\, sin\varphi\, cos\varphi \\ \varepsilon\, sin\varphi\, cos\varphi & \varepsilon\, sin^2\varphi \end{bmatrix}. \quad \text{(S10)}$$

The coordinate transformation is then:

$$\begin{bmatrix} x \\ y \end{bmatrix} = \begin{bmatrix} \varepsilon\, cos^2\varphi & \varepsilon\, sin\varphi\, cos\varphi \\ \varepsilon\, sin\varphi\, cos\varphi & \varepsilon\, sin^2\varphi \end{bmatrix} \begin{bmatrix} x_0 \\ y_0 \end{bmatrix} + \begin{bmatrix} x_0 \\ y_0 \end{bmatrix}. \quad \text{(S11)}$$

Thus, the transformed unit vectors pointing along the triclinic cell edges can be found by setting (1, 0) and (0, 1) in Eq. (S11):

$$\overrightarrow{b_1} = \frac{1}{\delta_X} \begin{bmatrix} 1 + \varepsilon\, cos^2\varphi \\ \varepsilon\, sin\varphi\, cos\varphi \end{bmatrix}, \quad \text{(S12)}$$

$$\overrightarrow{b_2} = \frac{1}{\delta_Y} \begin{bmatrix} \varepsilon\, sin\varphi\, cos\varphi \\ 1 + \varepsilon\, sin^2\varphi \end{bmatrix}, \quad \text{(S13)}$$

where

$$\delta_X = \sqrt{(1 + \varepsilon\, cos^2\varphi)^2 + \varepsilon^2 sin^2\varphi cos^2\varphi}, \quad \text{(S14)}$$

$$\delta_Y = \sqrt{(1 + \varepsilon\, sin^2\varphi)^2 + \varepsilon^2 sin^2\varphi cos^2\varphi}. \quad \text{(S15)}$$

For a simulation box of original in-plane dimensions L_X and L_Y, the new dimensions are $L_X\delta_X$ and $L_Y\delta_Y$. The angle between unit vectors is $\alpha = cos^{-1}(\overrightarrow{b_1} \cdot \overrightarrow{b_2})$. The transformed coordinates expressed in the triclinic system are $x_{tri} = \delta_X x$ and $y_{tri} = \delta_Y y$, and the new position vectors are $\vec{r} = x_{tri}\overrightarrow{b_1} + y_{tri}\overrightarrow{b_2}$ when expressed in the original coordinate system.

S5. Directional response for diamond-shaped and triangular pores

To better illustrate the symmetry observed in the response of permeability to uniaxial strains, an example of the full set of equivalent strain directions is shown in Fig. S7. In addition, we performed a directional strain sweep applied to nitrogen-terminated triangular pores in monolayer hexagonal boron nitride (hBN) [3, 4]. Note that all atomic charges were set to their

bulk values according to the recently reported parameterization [5] and thus the anisotropy here arises only from the pore geometry. The results are shown in Fig. S8; the observed anisotropy, although modest, exhibits symmetry similar to that observed for the diamond-shaped pores in MoS_2.

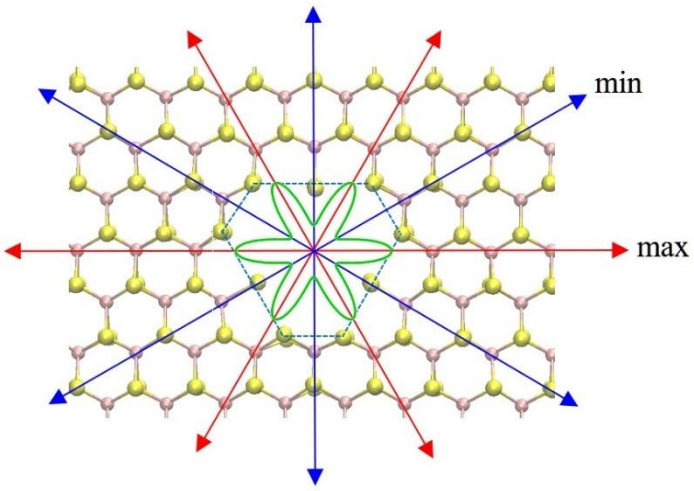

Figure S7. Diamond-shaped pore in MoS_2 and a complete set of equivalent directions corresponding to the angular response shown in Fig. 5 of the main text. The green "flower" corresponds to the sinusoidal data fit in Fig. 5. Note that for clarity the ~7-degree tilt in the response observed in Fig. 5 is omitted here. Blue and red arrows correspond to uniaxial strain directions with the minimal and maximal ionic currents, respectively.

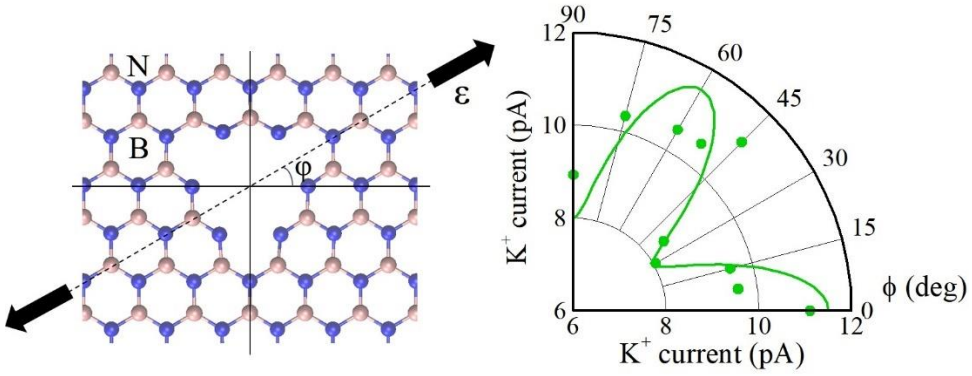

Figure S8. Single-pore K^+ currents across N-terminated triangular pores in monolayer hBN, as obtained from 0.5M aqueous KCl. Each permeation point was simulated for 400 ns. The directional strain sweeps were performed in the range $0° \leq \varphi \leq 90°$, as described in the main text. The average data uncertainty is 2 pA.

To demonstrate detection of parasitic pre-strain present in the membrane, we performed simulations similar to those presented in the main Fig. 5, except using a membrane, in which the pores are densely spaced and there is parasitic pre-strain ($\varepsilon \approx 0.01$) along the X-direction. The results of the angular sweep in Fig. S9, aside from revealing larger ionic currents than those in

Fig. 5, contain a significant symmetry distortion in the *Y-direction* in the corresponding permeability response.

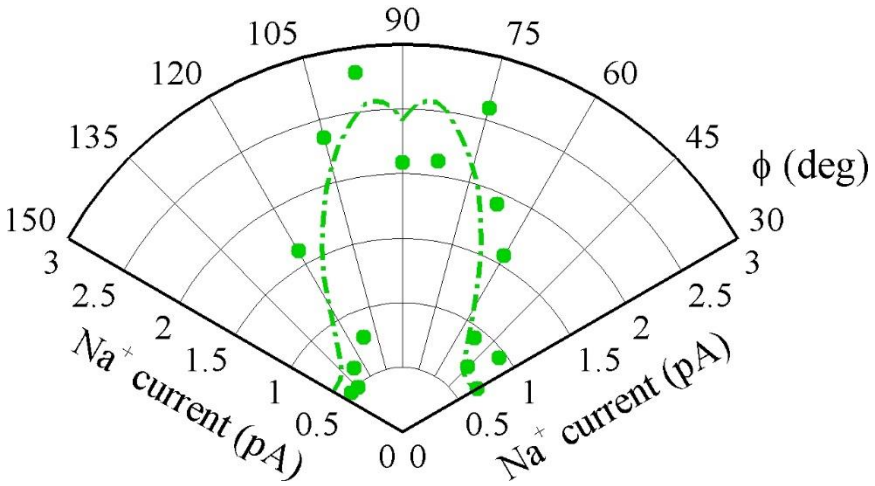

Figure S9. Response of Na^+ permeability to the angular sweep of uniaxial tensile strain ($\varepsilon = 0.04$), as applied to pre-strained pores. The angular range is $30° \leq \varphi \leq 150°$, roughly corresponding to twice the response period of the pores in Fig. 5 and Fig. S7. Each permeation point was simulated for 400 ns. The average data uncertainty is 0.2 pA.

S6. Temperature dependence of permeation anisotropy in N_4O_2 pores

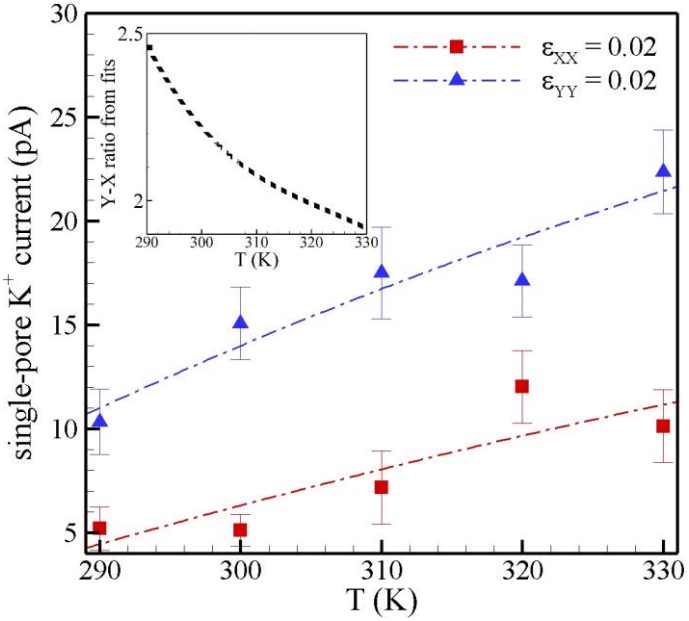

Figure S10. Single-pore K^+ currents across N_4O_2 pores subject to uniaxial strains $\varepsilon_{XX} = 0.02$ and $\varepsilon_{YY} = 0.02$ at various temperatures. The dash-dotted lines are quadratic fits to the ionic current data, used to obtain the trend in the resulting anisotropy ratio $\kappa_{YX} = I_{YY}/I_{XX}$ shown in the inset.

References

1. Fang, A., et al., *Highly mechanosensitive ion channels from graphene-embedded crown ethers.* Nature Materials, 2019. **18**(1): p. 76-81.
2. Politano, A. and G. Chiarello, *Probing the Young's modulus and Poisson's ratio in graphene/metal interfaces and graphite: a comparative study.* Nano Research, 2015. **8**(6): p. 1847-1856.
3. Cretu, O., et al., *Structure and Local Chemical Properties of Boron-Terminated Tetravacancies in Hexagonal Boron Nitride.* Physical Review Letters, 2015. **114**(7): p. 075502.
4. Gilbert, S.M., et al., *Fabrication of Subnanometer-Precision Nanopores in Hexagonal Boron Nitride.* Scientific Reports, 2017. **7**(1): p. 15096.
5. Govind Rajan, A., M.S. Strano, and D. Blankschtein, *Ab Initio Molecular Dynamics and Lattice Dynamics-Based Force Field for Modeling Hexagonal Boron Nitride in Mechanical and Interfacial Applications.* The Journal of Physical Chemistry Letters, 2018. **9**(7): p. 1584-1591.